

Use of the Correct Satellite Repeat Period to Characterize and Reduce Site-Specific Multipath Errors

Penina Axelrad, Kristine Larson, Brandon Jones
University of Colorado, Boulder

BIOGRAPHIES

Penina Axelrad is Professor of Aerospace Engineering Sciences with the Colorado Center for Astrodynamics Research at the University of Colorado, Boulder. Her research interests are in GPS technology and applications to aerospace systems. She has been involved in GPS work since 1985 and is a past president of the ION.

Kristine M. Larson received a B.A. in Engineering Sciences from Harvard and a Ph.D. in Geophysics from the University of California, San Diego. Her research focuses on high-precision applications of GPS, including plate tectonics, volcano monitoring, seismology, and time transfer. She is currently Professor of Aerospace Engineering Sciences at the University of Colorado.

Brandon Jones is a graduate student with the Colorado Center for Astrodynamics at the University of Colorado at Boulder. He previously worked as a contractor on GNC flight software development at NASA/JSC. His research interests include satellite orbit determination and GPS technology applications for satellite navigation.

ABSTRACT

Multipath caused by reflectors in the vicinity of GPS ground reference stations is a dominant error source in differential GPS and high rate precise positioning applications. Techniques for calibration and correction of these errors often rely on the repeatability of the GPS satellite geometry. While it is generally assumed that the repeat occurs at a time shift equal to the difference between the solar day and a sidereal day (23 hours, 56 minutes, 4 sec), the actual repeat shift is slightly different for each satellite, depending on its true orbital period. The average for the constellation is approximately 244 - 246 s (rather than 236 s) shy of 24 hours. The correct shift can be determined based on the broadcast ephemeris parameters or by comparing local geometry from day to day. This paper provides an overview of multipath effects on code, SNR, and carrier phase measurements including

expressions to estimate distance to the reflector for simple geometries. We then present several methods for computing the correct time shift for each satellite and apply these shifts to compare code and SNR observations from day to day. Results from three ground stations show a reduction in the code multipath when the observables are differenced from day to day. This has the potential to provide significant benefit for differential GPS, WAAS, JPALS, and common view time transfer.

INTRODUCTION

Satellite navigation signals reflected from surfaces near a user antenna interfere with direct signals, producing multipath errors in the measurement of pseudorange (code), carrier phase, and signal-to-noise ratio (SNR). The level of interference depends on the reflective properties of the surface and its distance from the antenna. The resulting measurement errors depend on the receiving antenna pattern, receiver front-end bandwidth, and the tracking loop design. Many innovative hardware and signal processing approaches have been developed to reduce the sensitivity of receivers to multipath signals [c.f. 1-8] and measurement smoothing schemes are employed to further reduce its influence [9-11]. Despite these efforts and because of continuous improvements in reducing other sources of error in GNSS, multipath errors remain the dominant error source for most fixed sites.

The signature feature of multipath is an oscillation that occurs in all three observation types. The amplitude of the multipath induced errors in carrier phase observations is limited to a quarter wavelength or about 5 cm, but is typically well below 2 cm. Code multipath can be quite large because it depends directly on the distance to the reflector. Thus, one approach to reducing code multipath is simply to apply carrier smoothing to code observations. This approach is quite effective in the absence of cycle slips and loss of carrier lock. Calibration of multipath errors has also been described for various applications [c.f. 12-16]. These approaches rely on making repeatable measurements of multipath.

For differential reference stations it is very desirable to remove multipath from the observed pseudoranges to reduce the impact of this error on users. In 1994, Bishop, *et al.* [12] developed a multipath template approach, wherein code errors on one day were identified and used to correct measurements on subsequent days. They correctly recognized the shortcomings of assuming a perfect sidereal day shift of the results and also looked at the spatial variability of the template. The analysis presented here further quantifies these effects and presents results from additional sites and receiver types. Repeatability has also been exploited to reduce multipath in geophysical applications through the use of sidereal filtering [17, 18]. As described by Choi, *et al.* [18], this is more effective when the correct satellite time shift is used.

This paper first presents an overview of multipath models and the manifest errors. These models permit a specification to be set on the degree of repeatability required to provide a benefit in reducing fixed site pseudorange errors. An evaluation of the GPS satellite repeatability is then presented and the use of correction profiles to reduce code multipath is demonstrated.

MULTIPATH MODELS

Figure 1 illustrates the simplified geometry for a fixed antenna and a large tilted planar reflector at a distance, h , from the surface. The angle of incidence of the signal with respect to the reflector plane is γ and the angle of the plane with respect to the local level is β . Because the GPS satellites are very distant, all lines of sight can be considered parallel.

The reflected signal arrives at the antenna delayed, phase-shifted, and attenuated with respect to the direct signal. These modifications are described by three parameters:

- δ – additional path length with respect to the direct
- ψ – phase shift with respect to the direct
- α – ratio of the signal amplitude of the reflection to that of the direct

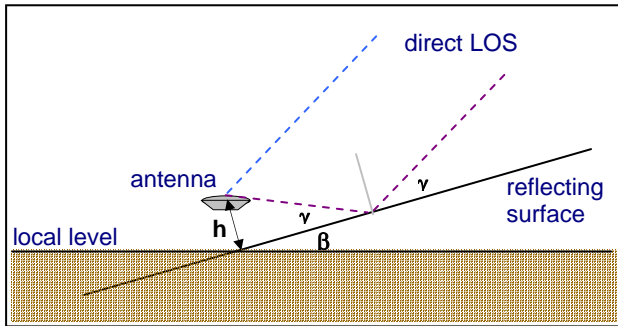


Figure 1. Simplified reflector geometry. The antenna is at a distance h , normal to the surface. The satellite line of sight is incident at angle, γ , to the surface.

The multipath phase shift is equal to the path delay converted to radians with a possible offset,

$$\psi = 2\pi \frac{\delta}{\lambda} + \psi_0. \quad (1)$$

Many references have developed expressions for the measurement errors produced by multipath [c.f. 19-22]. The most complete models include features of the tracking loops. However, for this analysis it is sufficient to consider only the most basic model assuming no coupling between the code and carrier loops, and coherent tracking of carrier. Figures 2 and 3 illustrate the simple model of direct and reflected signal components in the carrier phase plane and code correlation function, respectively.

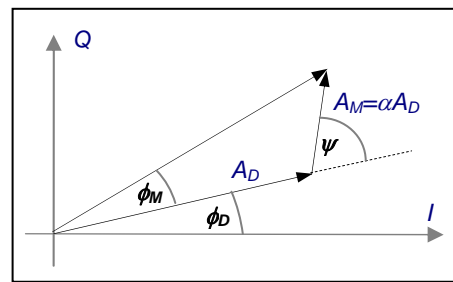


Figure 2. Effect of multipath on carrier phase.

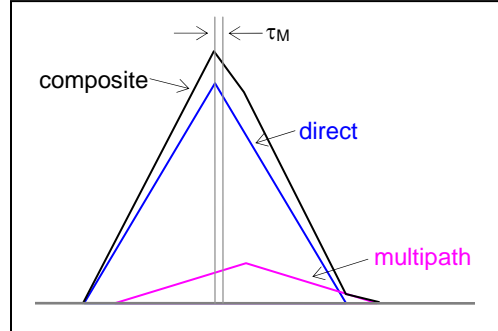


Figure 3. Effect of multipath on code measurement. The code tracking error is τ_m .

The carrier tracking loop produces measurements of amplitude or signal to noise ratio (SNR) and phase of the composite signal given by SNR_C and ϕ_C , that differ from the measurements of the direct signal SNR_D and ϕ_D due to multipath. The SNR due to multipath is given by,

$$SNR_M = \alpha^2 A_D^2 + \alpha 2 A_D^2 \cos \psi \quad (2)$$

and the phase error due to multipath by,

$$\tan \phi_M = \frac{\alpha \sin \psi}{1 + \alpha \cos \psi}. \quad (3)$$

The pseudorange error due to multipath, τ_M , is implicit in the ideal code tracking loop discriminator equation,

$$\begin{aligned} & [R(\tau_M + T_{E/L}) - R(\tau_M - T_{E/L})] \\ & + \alpha [R(\tau_M + T_{E/L} - \delta) - R(\tau_M - T_{E/L} - \delta)] \cos \psi = 0 \end{aligned}$$

where $2T_{E/L}$ is the early/late discriminator spacing, R is the autocorrelation function of the code, and the carrier tracking error is assumed to be zero. If we assume an ideal triangular autocorrelation function,

$$R(\tau) = 1 - \frac{|\tau|}{T} \text{ for } |\tau| < T \quad (4)$$

and a short delay multipath $\delta < T_{E/L}$, this can be solved explicitly for the code multipath error as,

$$\tau_M = \frac{\alpha \delta \cos \psi}{1 + \alpha \cos \psi}. \quad (5)$$

Notice that for small multipath amplitudes this error is in phase with the SNR oscillations and proportional to the additional path length, δ . This dependence on additional path length is important because it means that locating a reference antenna farther away from a potential reflector, for example on top of a tall pole above a reflective ground surface, may, in fact have a detrimental effect on the code measurements. The same is not true for the carrier phase measurements; which are not influenced directly by the magnitude of the path delay, but rather, only by its value modulo the wavelength.

In analyzing experimental data it is common to estimate the code multipath error based on the difference between the code and carrier phase observations, corrected for ionospheric delay. This code multipath observable is computed from the measured pseudorange ρ_1 and phase on both L1 and L2 (ϕ_1 and ϕ_2) and is related to the code multipath error (τ_M as follows):

$$\begin{aligned} MP_1 &= \rho_1 - \frac{f_1^2 + f_2^2}{f_1^2 - f_2^2} \phi_1 \lambda_1 + \frac{2f_2^2}{f_1^2 - f_2^2} \phi_2 \lambda_2 \\ &= \tau_M + C + \varepsilon_\rho \end{aligned} \quad (6)$$

where C is a constant due to the integer ambiguity in the two phase measurements and ε_ρ is the code tracking noise.

Since the influence of multipath on all three measurements is dominated by a sine or cosine of the phase shift, ψ , to understand the periodicity of multipath we need only look at the rate of change of ψ .

In a dynamic environment, ψ may change due to motions of the reflectors relative to the antenna, but for a static antenna and unchanging environment, multipath phase delay changes only due to motion of the satellites. For a simple planar reflector as shown in Figure 1, the additional path length of the specular reflection with respect to the direct is given by:

$$\delta = 2h \sin \gamma \quad (7)$$

and the corresponding phase delay of the reflected signal is,

$$\psi = 2\pi \cdot \frac{2h \sin \gamma}{\lambda} + \psi_0 = 4\pi \frac{h}{\lambda} \sin \gamma + \psi_0 \quad (8)$$

again, with a possible fixed offset (ψ_0) due to a phase shift at the reflecting surface.

To understand multipath oscillations we look at the time rate of change of ψ , which corresponds to the rate at which the reflected signal phasor spins around the tip of the direct signal phasor in Figure 2.

For the planar reflector, we have

$$\frac{d\psi}{dt} = 4\pi \frac{h}{\lambda} \frac{d}{dt} (\sin \gamma) = 4\pi \frac{h}{\lambda} \cos \gamma \frac{d\gamma}{dt} \quad (9)$$

From this equation it is apparent that for small incidence angles there is a faster multipath phasor spin for the same angular change in incidence than for large incidence angles. For an antenna above a horizontal ground plane, this results in fast multipath oscillations at low elevations and very slow changes at high elevations.

We can eliminate the time varying effect by directly considering the rate of change of ψ with respect to $\sin \gamma$. Defining the independent variable to be,

$$x = \sin \gamma$$

we find that

$$\frac{d\psi}{dx} = 4\pi \frac{h}{\lambda} = 2\pi \frac{2h}{\lambda}. \quad (10)$$

One can think of $2h/\lambda$ as the spatial frequency, f_M , of the multipath measured in cycles per full satellite arc from 0 to 90 degrees. So if the spatial frequency is measured, the simple planar reflector distance can be computed as:

$$h = \frac{1}{2} f_M \lambda. \quad (11)$$

This relationship also permits the reflector distance h , to be estimated from the number of multipath-induced

oscillations, n_M over a satellite arc ranging from γ_{\min} to γ_{\max} as follows:

$$h = \frac{\lambda n_M}{2(\sin \gamma_{\max} - \sin \gamma_{\min})} \quad (12)$$

Figure 4 gives an example of code multipath for two satellites (PRN 23 and 31) during a pass from 15 to 20 deg elevation, measured at the Goldstone IGS Site (GOLD) shown in Figure 5 [23]. A count of cycles in these plots is estimated at 20-23 cycles, yielding a height estimate of 23-26 meters above the ground. The GOLD antenna height is known to be approximately 25 m above the ground [23]. Counting of cycles is only feasible in situations where a large dominant reflector drives the multipath for a region of the sky. Figure 6 shows the same satellites and elevation range measured at the SCIGN Site (POMM) shown in Figure 7 [24]. In this case we see substantially different oscillations in the same elevation angle range. This is indicative of structures other than the ground being responsible for the multipath.

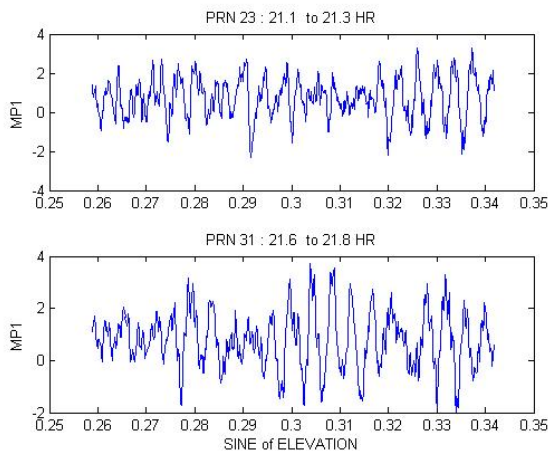


Figure 4. Code multipath observable for PRNs 23 and 31 at Goldstone on DOY 272, 2004, as a function of sine of elevation angle.

It is clear that the simplified plate model does not apply directly in many situations. Fortunately, we can take advantage of the repeatability of multipath even in complex simulations. To be most effective, it is important to quantify exactly how repeatable the geometry is.



Figure 5. Photograph of IGS Goldstone Antenna Installation. According to the site log, the GPS antenna is mounted on top of a 25 meter, unguided Microwave tower, within 100 meters of the MARS 70 meter diameter Deep Space Antenna [23].

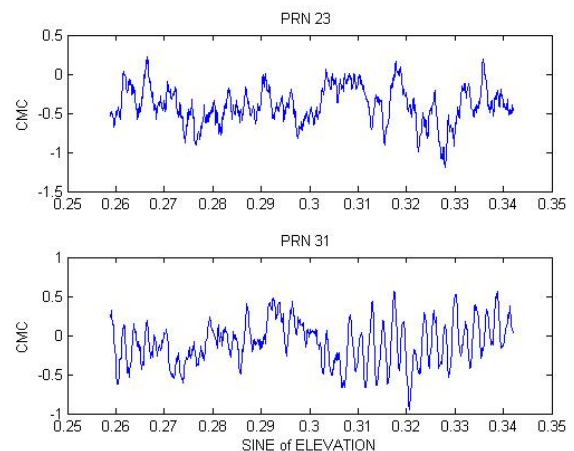


Figure 6. Code multipath observable for PRNs 23 and 31 at POMM on DOY 272, 2004, as a function of sine of elevation angle.



Figure 7. POMM Photograph (Courtesy J. Langbein)

Equation (9) permits an estimate to be made of how closely aligned the antenna/satellite geometry must be to produce a correlated multipath error. If the maximum allowable change in phase is given by $\Delta\psi$, the maximum permissible change in incidence angle is computed from:

$$\Delta\gamma_{\max} = \frac{\Delta\psi_{\max} \lambda}{4\pi h \cos \gamma} \geq \frac{\Delta\psi_{\max} \lambda}{4\pi h}. \quad (13)$$

So, for an allowable path delay shift of $\pi/8$ (22.5 deg), a conservative bound on the angular repeatability is 1.8 deg for a reflector at a distance of 1λ (~19 cm), 0.34 deg for a reflector at a 1 m distance, or 0.034 deg for a reflector at a 10 m distance. Thus, if an antenna is located in an environment with distant reflectors, correction profiles and correction maps must be generated with the appropriate angular spacing.

As an example, Reference 16 describes experiments with a multipath calibration system in which very rapidly varying multipath errors were observed. Based on the analysis presented here, it appears that distant reflectors are likely to be the source of the observed effect. Conversely for GPS installations on a small spacecraft, such as that evaluated in [14] the spatial frequencies and corresponding required calibration grid resolution are lower because no distant surfaces exist.

REPEATABILITY

It is well known that the GPS satellite orbits were selected to have a period of one half a sidereal day (23 h 56 m 4 s) with a daily repeating ground track. Because of this choice, satellite visibility from any point on earth is the same from day to day, with the satellites appearing in their positions approximately 4 minutes (236 s) earlier each day due to the difference between the sidereal and solar day. This was a useful property especially in the early days of GPS when session planning was important to insure adequate satellite coverage. With the easily predictable coverage, GPS users could plan repeatable campaign times well in advance just by shifting their experiments forward each day by 4 minutes.

Operationally, the GPS satellite orbit specification is put on the repeatability of the longitude of the ascending node which is kept within ± 2 deg of a nominal value. This essentially constrains the ground track of the satellite to repeat to within about ± 222 km. When a satellite orbit goes outside this range, an orbit adjustment is made by the control segment [25].

For a purely Keplerian orbit the repeating ground track can be established by setting the semimajor axis of the orbit such that the period of motion equals one half the sidereal day:

$$P = 2\pi\sqrt{a^3/\mu}$$

$$a_{\text{repeat}} = \left[\mu \left(\frac{\frac{1}{2} P_{\text{sidereal}}}{2\pi} \right)^2 \right]^{1/3} = 26,561.74 \text{ km}$$

In reality, perturbations of the orbit are caused by the non-central gravity field of the earth, the gravitational attraction of the sun, moon, and other planets, solar radiation pressure and atmospheric drag. Estimates of these influences at the GPS altitude are given by Spilker [26]. Earth oblateness has the largest effect on the ground track repeat at the GPS orbit altitude, producing a secular nodal drift of westward by 14.665 deg per year [25]. To compensate for this motion of the orbit plane, the average semimajor axis of the GPS satellite orbits is set slightly low such that the orbital period is about 4 s faster than a sidereal half-day and consequently the time shift of the daily repeat for most satellites in the constellation is closer to 244 s.

Three methods are evaluated for estimating the correct daily shift of the GPS satellite geometry: 1) compute the period from the semimajor axis given in the broadcast ephemeris or almanac data; 2) compute the repeat time by interpolating precise orbits to the time of equator crossings; and 3) find the actual repeat geometry for a selected location and identify the associated time shift.

The simplest method for estimating the shift is based on the broadcast almanac or ephemeris parameters. The semimajor axis-based shift (T_a) is computed as follows:

$$T_a = 86400 - 2(2\pi/n) \quad (14)$$

where the mean motion, n , is given by,

$$n = \sqrt{\mu_E/a^3} + \Delta n \quad (15)$$

and a and Δn are the semimajor axis and mean motion adjustment, respectively, defined in the broadcast ephemeris message, and μ_E is the gravitational constant of the earth specified as $3.986005 \times 10^{14} \text{ m}^3/\text{s}^2$ for use with the broadcast elements.

Figure 8 gives the T_a shift computed on a daily basis for most satellites in the GPS constellation during 2004 using average of the all the daily broadcast elements. These satellites are seen to have a typical shift of 244 s with a small secular drift due to a near resonance of the GPS orbits with the tesseral harmonics of the Earth's field, plus small amplitude variations occurring twice monthly due to lunar perturbations of the orbits. Abrupt steps in the time shift are due to satellite orbit maintenance maneuvers which can be identified in the NANUs [27]. Figure 9 shows two satellites (PRN 1 and 31) which were subject to some significant maneuvering, and in effect did not execute precisely repeating orbits for part of the year.

Table 1. GPS Orbital Plane Assignments in 2004.

PLANE	PRNS				
A	9	25	8	27	
B	16	30	28	5	
C	6	3	19	7	31*
D	2*	11	21	4	15 24*
E	20	22*	10	18	18
F	14	26	13	23*	29 1*

* Indicates a satellite that had significant maneuvers in 2004 and is not shown in Figure 8.

A second approach to checking repeatability is to interpolate post-processed GPS orbit solutions to the equator crossing on subsequent days and find the associated time shifts (T_{equ}). The precise orbits are available from the IGS in SP3 files at 15 min intervals and can be interpolated to the equator crossing using a Lagrangian interpolator [28]. We found that this method produced time shifts that are within 0.2 sec of the values computed based on the broadcast ephemeris parameters.

The third approach considered is based on local geometry; thus it is the most relevant for ground station multipath repeatability but not as easy to implement as the previous methods. The objective is to find for each measurement epoch on one day, the measurement epoch on the preceding day that corresponds most closely to the same geometry. This can be determined by finding the time shift which maximizes the dot product of the two user-to-satellite line of sight vectors (i.e. the cosine of the angle between them). We refer to this time shift based on geometry as T_g . For reference, the line of sight unit vector \hat{e} , expressed in the East-North-Up frame, can be computed based on the azimuth and elevation as:

$$\hat{e} = \cos(el)\sin(az)\hat{E} + \cos(el)\cos(az)\hat{N} + \sin(el)\hat{U} \quad (16)$$

Figures 10 and 11 show satellite passes for two satellites on two subsequent days illustrating the angular separation of the closest points and giving the time varying time shift corresponding to these points. (The short gaps in the graphs are due to data outages on DOY 273.) Satellite orbits that are farthest from having a truly repeating ground track tend to have the largest variation in time shift during a single pass. Satellites with ground tracks that are very close to overlapping have essentially constant time shifts. The shifts are quantized at the level of 1 s and the small jumps for a few points are due to the data outages.

Table 2 gives a comparison of T_a and the range of T_g at Goldstone for all GPS satellites comparing DOY 272 to 273, 2004. (Shifts associated with measurement gaps are not included in the T_g range.)

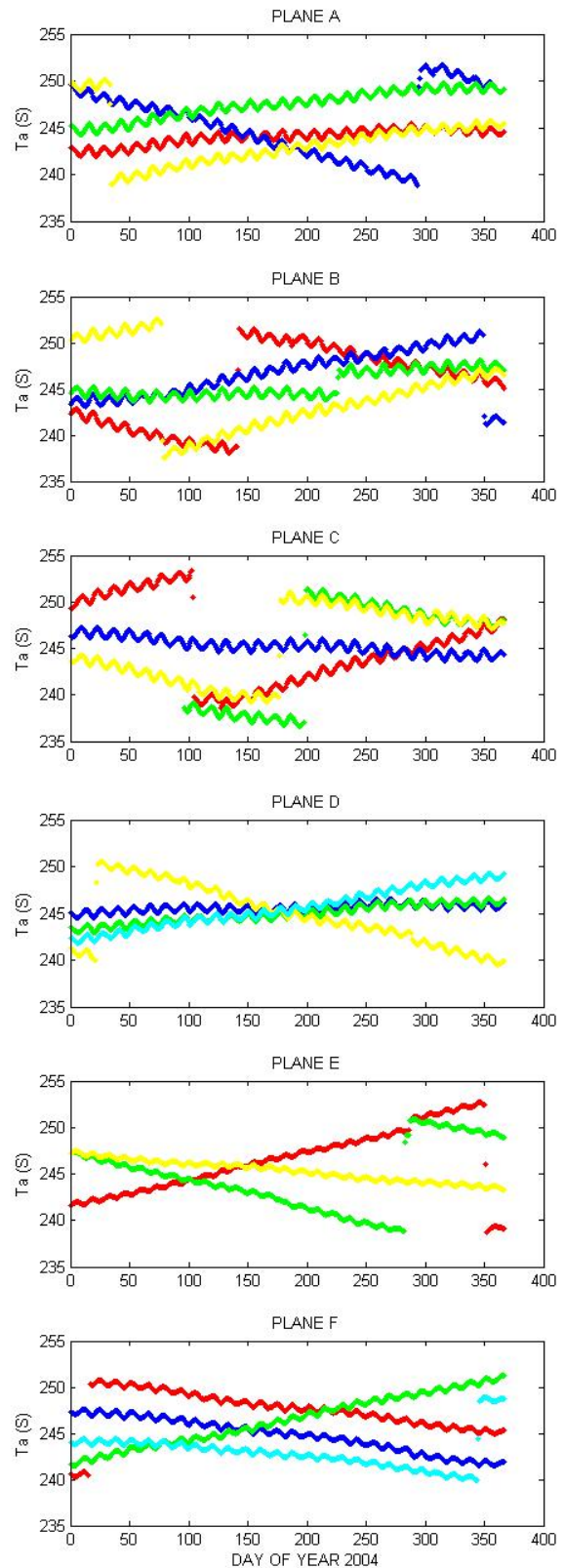


Figure 8. Shift of GPS satellite geometry based on broadcast ephemeris data for 2004. Satellites are grouped by their orbital plane assignments. Satellites with unusual periods (shown with * in Table 1) are not included here.

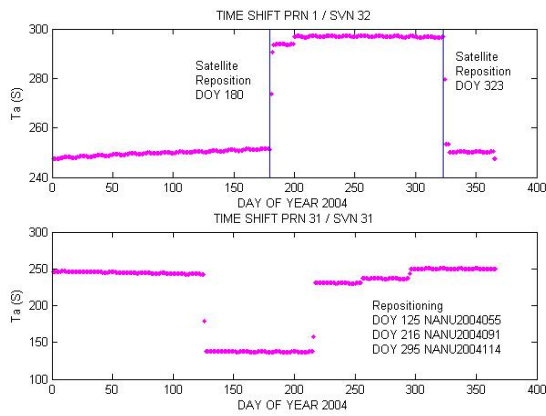


Figure 9. Time shifts for PRNs 1 and 31 in 2004. Note that because these shifts are so large, the satellite orbits are not very repeatable.

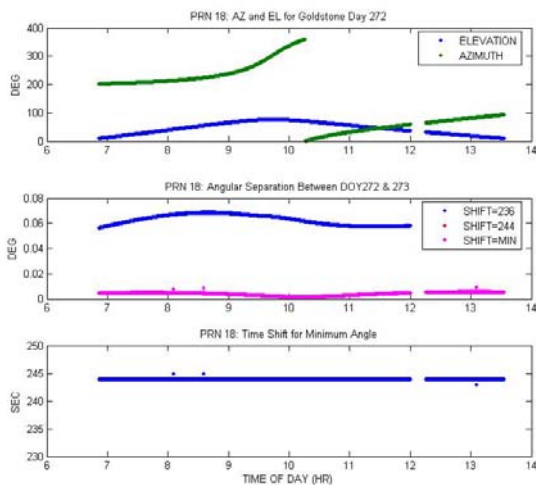


Figure 10. Geometrical repeat for PRN 18 at Goldstone on DOY 272 & 273, 2004. The top figure shows the azimuth and elevation track of the satellite as seen from Goldstone. The middle plot shows the angular separation between the line of sight vectors on DOY 273 compared to DOY 272 using the sidereal time shift of 236 s, the orbit based shift of 244 s for this satellite, and the closest geometry time shift (the latter two are almost identical). The bottom graph shows the time varying time shift for closest geometry. For this satellite the repeat is very close to 244 s throughout the pass.

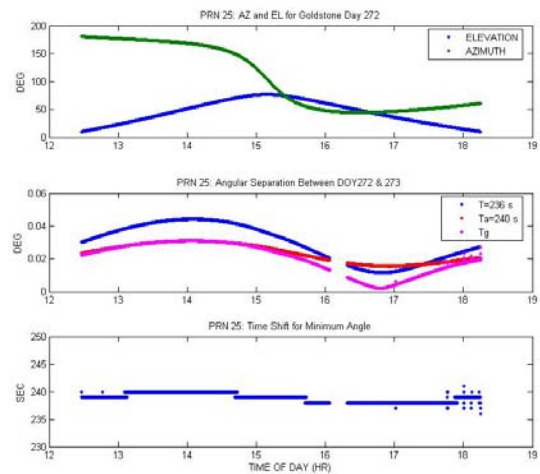


Figure 11. Geometrical repeat for PRN 25 at Goldstone on DOY 272 & 273, 2004. The top figure shows the azimuth and elevation; middle plot shows the angular separation and the bottom graph shows the time varying time shift for closest geometry.

Table 2. Time shifts for DOY 272 to 273 based on broadcast ephemeris and geometry at Goldstone.

PRN	Ta (s)	Tg (s)	PRN	Ta (s)	Tg (s)
1	297	298-318	18	244	244
3	245	244-245	19	249	249-250
4	243	240-244	20	249	250-252
5	244	242-244	21	246	246
6	244	243	22	245	245
7	249	249-251	23	242	239-241
8	249	249-251	24	244	243-244
9	245	245	25	240	238-240
10	239	236-238	26	244	243
11	247	246-247	27	245	245
13	249	249-251	28	247	247
14	247	247	29	241	240-241
15	248	248-249	30	249	249-250
16	248	248-249	31	237	242-243
17	246	246			

MULTIPATH REPEATABILITY

To investigate multipath repeatability for a fixed ground site we look at the code multipath for three sites – Goldstone and Pomm described previously, and the roof of the CU Engineering Center (ROOF). Both GOLD and POMM are designed as reference station locations whereas ROOF represents a poor antenna installation in the vicinity of many potential reflecting surfaces.

Figure 12 shows MP1 and SNR for PRN 18 at Goldstone on DOY 272 as a function of time of day. In this broad view we can see that the multipath errors are quite large and the SNR is dominated by the antenna pattern with high frequency fluctuations superimposed. In Figure 13, the first and third graphs show MP1 for the two time segments of DOY 272 and 273 during which the satellite elevation is between 10-30 degrees. The standard deviation of MP1 is also given for each day. It is clear that the MP1 values are highly correlated and shifted in time.

Because of this high degree of repeatability one would expect it to be possible to subtract a multipath profile derived one day from the subsequent day's observations to improve the code measurement accuracy. The second and fourth graphs in Figures 13 show the difference between MP1 values on the two days when shifted by the sidereal shift T_s of 236 s, the computed semimajor axis shift T_a , and the computed optimal geometric shift T_g . Standard deviations are shown as well. For both segments shown, the differenced MP is reduced compared with the individual day values if T_a or T_g is applied. The application of T_s does not yield satisfactory results.

It is clear from this result that applying the correct time shift is crucial to exploiting multipath repeatability. It is also noteworthy that high rate data are required because measurements spaced at 30 s or even 5 s cannot be properly aligned to ensure sufficient multipath correlation. This is particularly apparent at Goldstone because of its high mounting location, but the value of high rate data should be considered for any installation.

Figures 14-15 provide additional illustrations and summaries of multipath reduction at GOLD and POMM using both T_a and T_g shifts. In Figure 15 the standard deviation of the T_a -shifted multipath difference between days 272 and 273 is plotted against the standard deviation of multipath for a single day, for each 10-30 elevation range pass (excluding PRN 1 which was not in a sufficiently repeatable orbit). Points that lie below the diagonal line represent improvements due to the daily filtering. The few points above the line represent arcs that would be degraded by daily differencing. It is possible that these RMS values include the result of undetected cycle slips in the MP1 observable.

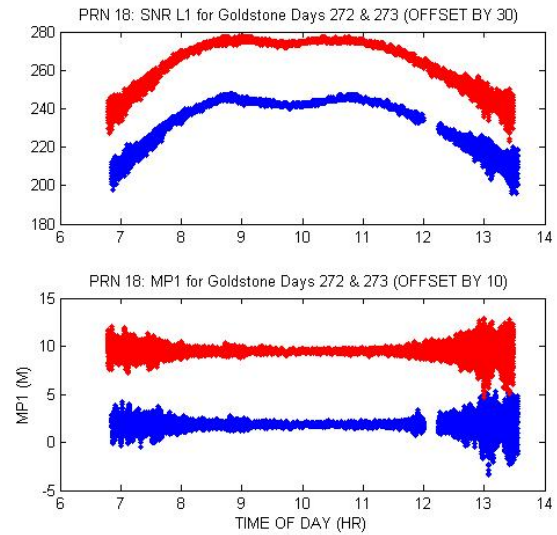


Figure 12. MP1 and SNR for PRN 18 at Goldstone DOY 272 (blue) and DOY 273 (red). The curves are offset from each other for clarity.

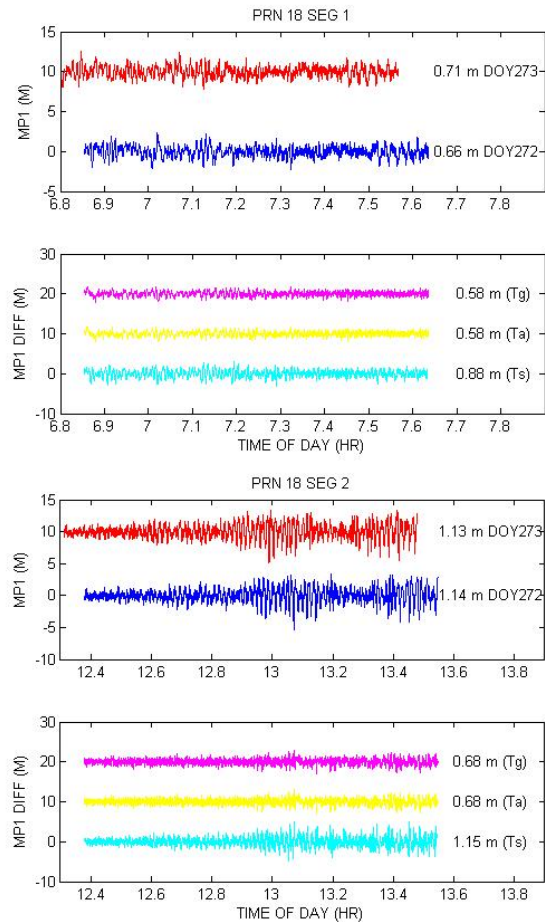


Figure 13. MP1 for PRN 18 Segments 1 and 2 at Goldstone. The first and third graph give the MP1 measurements on each day. The second and fourth graphs show the difference in MP1 when time shifted by T_s , T_a , and T_g . The curves are offset from each other for clarity.

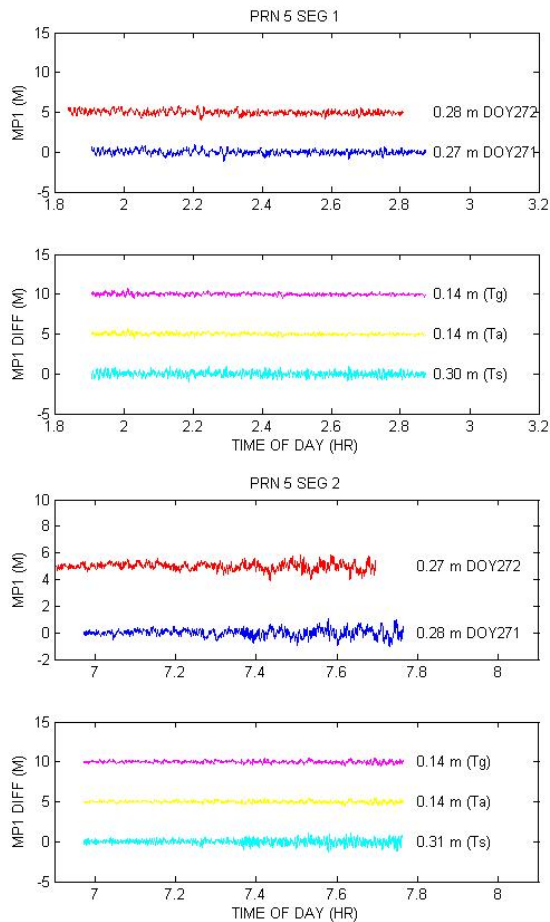


Figure 14. Code multipath for PRN 5 at POMM, DOY 271 and 272, 2004 in elevation range of 10-30 deg.

Figure 16 shows an aerial photograph of the CU Engineering Center rooftop used for multipath experiments. The data presented were recorded by a narrow correlator NovAtel OEM 4 dual frequency receiver with a Pinwheel L1/L2 antenna. Figure 17 shows the MP1 observable on DOY 259 and 260 of 2004 and the difference in the T_a -shifted observables. These illustrate that despite the complex rooftop environment, the multipath is highly repeatable.

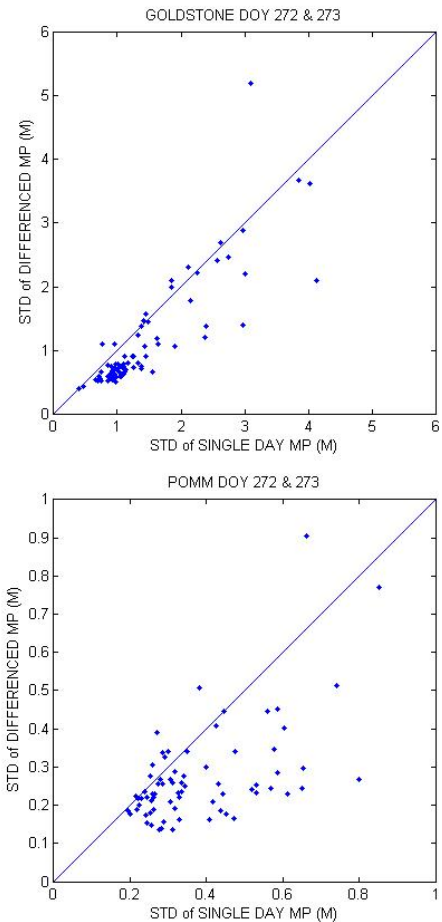


Figure 15. Comparison of MP1 for individual days to differenced MP1 at GOLD (top) and POMM (bottom). Each point represents the MP statistics over a single 10-30 deg pass. The x-axis value is the standard deviation of the single day MP and the y-axis value is the standard deviation of the MP differences shifted by T_a .



Figure 16. Aerial photo of Engineering Center. The blue circle marks the approximate location of the antenna.

Because of the high frequency oscillations present in the MP1 for PRN 16, it is particularly sensitive to the correct daily time shift. For the segment of PRN 16 shown, the multipath difference increases from 6 cm to 20 cm if the sidereal time shift is applied rather than the computed T_a of 248 s. For PRN 27, which has smaller amplitude and lower frequency oscillations, the increase is not significant (6 cm to 7 cm) between the actual T_a of 244 s for this satellite and the standard T_s of 236 s.

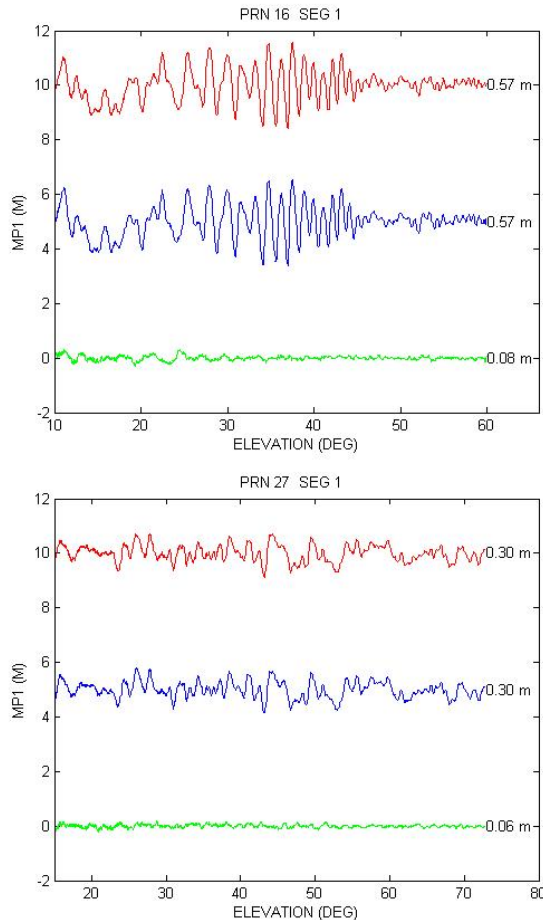


Figure 17. MP1 and Difference in MP1 for Roof DOY 259 and 260, 2004, PRNs 16 and 27. The red, blue, and green lines show DOY259, DOY260, and the T_a -shifted difference, respectively.

CONCLUSIONS

The models, algorithms, and results presented here provide a basis for computing and applying daily filters to ground reference station code measurements. It is seen that the frequency content of the GPS observations can be used to identify the approximate distance to potential reflectors and to specify repeatability or grid spacing requirements for multipath calibration and correction. It was also demonstrated that complex environments can

demonstrate highly repeatable multipath when satellite geometry is carefully accounted for.

To apply this work to reference station installations a number of logistical issues should be addressed, specifically the length and elevation range of arcs to be applied, and the detection and correction of carrier phase cycle slips in the construction of the code multipath observable.

ACKNOWLEDGMENTS

The authors are grateful to John Langbein for providing the photographs of POMM, to James Gidney and John Berg for helpful discussions on the GPS orbits, to Ben Harris for recommending a key reference, and to our colleagues Andria Bilich, Steve Anderson, Jan Weiss, and Stephan Esterhuizen at the University of Colorado for their assistance in this work.

REFERENCES

1. Tranquilla, J.M, J.P. Carr, and H.M. Al-Rizzo, "Analysis of a Choke Ring Groundplane for Multipath Control in Global Positioning System (GPS) Applications," *IEEE Transactions on Antennas and Propagation*, 1994, Vol. 42, No. 7, pp. 905-911.
2. Van Dierendonck, A. J., Fenton, P., Ford, T., "Theory and Performance of Narrow Correlator Spacing in a GPS Receiver," *Navigation*, Vol. 39, No. 3, Fall 1992, pp. 265-283.
3. Townsend, B., P. Fenton, and K. Van Dierendonck, "Performance Evaluation of the Multipath Estimating Delay Lock Loop," *Navigation*, Vol. 43 No. 3, 1995, pp. 503-514.
4. Ray, J., M.E. Cannon, P. Fenton, "GPS Code and Carrier Multipath Mitigation Using a Multiantenna System," *IEEE Transactions on Aerospace and Electronic Systems*, Vol. 37, No. 1, 2001.
5. Brown, A. and N. Gerein, Test Results from a Digital P(Y) Code Beamsteering Receiver for Multipath Minimization," *ION 57th Annual Meeting*, Albuquerque, NM, June 2001.
6. Thornberg, D.B., D.S. Thornberg, M.F. DiBenedetto, M.S. Braasch, F. van Graas, and C. Bartone, "LAAS Integrated Multipath-Limiting Antenna," *Navigation*, Vol. 50 No. 2, 2003, pp. 117-130.
7. Weill, Lawrence. "Achieving Theoretical Accuracy Limits for Pseudorangeing in the Presence of Multipath," *ION GPS 1995*.

8. Zhdanov, Alexey; Veitsel, Victor; Zhodzinsky, Mark; Ashjaee, Javad, "Multipath Error Reduction in Signal Processing," *ION GPS 1999*, 14-17 September 1999, Nashville, TN.
9. Hatch, R. "The synergism of GPS code and carrier measurements," *Proceedings of the Third International Geodetic Symposium on Satellite Doppler Positioning*, Las Cruces, NM, 1982, pp. 1213 – 1232.
10. Hwang, P.Y., G.A. McGraw, J.R. Bader, "Enhanced Differential GPS Carrier Smoothed Code Processing Using Dual Frequency Measurements," *Navigation*, Vol. 26, No.2, 1999, pp. 127-137.
11. McGraw, G.A. and R.S.Y. Young, "Dual Frequency Smoothing DGPS Performance Evaluation Studies," *ION National Technical Meeting 2005*, 24-26 January 2005, San Diego, CA, pp. 170-181.
12. Bishop, G., D. Coco, P. Kappler, and E. Holland, "Studies and Performance of a New Technique for Mitigation of Pseudorange Multipath Effects in GPS Ground Stations," *ION National Technical Meeting 24-26 January 1994*, San Diego, CA, pp. 213-242.
13. Kee, C. and B. Parkinson, "Calibration of Multipath Errors on GPS Pseudorange Measurements," *ION GPS 1994*.
14. Reichert, A.K. and P. Axelrad "Carrier-Phase Multipath Corrections for GPS-Based Satellite Attitude Determination," *Navigation*, Vol 48. No.2, 2001, pp. 77-88.
15. Harris, R.B., "Evaluation, Refinement and Fusion of Software-Based Pseudorange Multipath Mitigation Techniques," *ION GPS 2002*, 24-27 September 2002, Portland, OR, pp. 460-471.
16. Park, K.-D., P. Elosegui, J. L. Davis, P. O. J. Jarlemark, B. E. Corey, A. E. Niell, J. E. Normandeau, C. E. Meertens, and V. A. Andreatta, "Development of an antenna and multipath calibration system for Global Positioning System sites," *Radio Science*, 39, (2004), RS5002, doi:10.1029/2003RS002999.
17. Genrich, J. F., and Y. Bock (1992), Rapid resolution of crustal motion at short ranges with the Global Positioning System, *Journal of Geophysical Research*, Vol. 97, pp. 3261–3269.
18. Choi, K., A. Bilich, K.M. Larson, and, P. Axelrad, "Modified Sidereal Filtering: Implications for High-Rate GPS Positioning," *Geophysical Research Letters*, Vol. 31, No. 22, 2004.
19. Braasch, M. S., "Multipath Effects," in *Global Positioning System: Theory and Applications, Volume 1*, B. W. Parkinson, J. J. Spilker Jr., P. Axelrad, P. Enge, ed., American Institute of Aeronautics and Astronautics, 1995.
20. Elosegui, P., J.L. Davis, R.T.K. Jaldehag, J.M. Johansson, A.E. Niell, and I.I. Shapiro, "Geodesy Using the Global Positioning System: The Effects of Signal Scattering on Estimates of Site Position," *Journal of Geophysical Research*, Vol. 100, No. B7, pp. 9921-9934, 1995.
21. Hannah, B.M., *Modelling and Simulation of GPS Multipath Propagation*, Ph.D. Dissertation, Queensland University of Technology, March 2001.
22. Ray, Jayanta K.; Cannon, M. Elizabeth. "Synergy Between Global Positioning System Code, Carrier, and Signal-to-Noise Ratio Multipath Errors," *Journal of Guidance, Control, and Dynamics*, Vol. 24, No. 1, Jan-Feb 2001.
23. International Geodynamics Service (IGS) <http://igsceb.jpl.nasa.gov/network/site/gold.html>.
24. Southern California Integrated GPS Network (SCIGN) www.scign.org.
25. Chao, C., and D. L. Schmitt, "Eliminating GPS stationkeeping maneuvers by changing the orbital altitude," *Journal of the Astronautical Sciences*, 39(2), 1991.
26. Spilker, J.J., "GPS Navigation Data," in *Global Positioning System: Theory and Applications, Volume 1*, B. W. Parkinson, J. J. Spilker Jr., P. Axelrad, P. Enge, ed., American Institute of Aeronautics and Astronautics, 1995, p. 169.
27. U.S. Coast Guard Notice Advisory to NAVSTAR Users (NANU) http://www.navcen.uscg.gov/gps/nanu_abbreviations.htm
28. Schenewerk, "A Brief Review of Basic GPS Orbit Interpolation Strategies," *GPS Solutions*, Vol. 6, No. 4, 2003, pp. 265-267.